Advances on creep-fatigue damage assessment in notched components

Daniele Barbera[1], Haofeng Chen[1*], Yinghua Liu[2]

[1]*Department of Mechanical & Aerospace Engineering, University of Strathclyde, Glasgow, G1 1XJ, UK*
[2]*Department of Engineering Mechanics, Tsinghua University, Beijing, 100084, China*

[*]*Corresponding author email: haofeng.chen@strath.ac.uk*

Abstract

In this paper, the extended Direct Steady Cyclic Analysis method (eDSCA) within the Linear Matching Method Framework (LMMF) is combined with the Stress Modified Ductility Exhaustion method and the modified Cavity Growth Factor (CGF) for the first time. This new procedure is used to systematically investigate the effect of several load parameters including load level, load type and creep dwell duration on the creep-fatigue crack initiation process in a notched specimen. The results obtained are verified through a direct comparison with experimental results available in the literature demonstrating great accuracy in predicting the crack initiation life and the driving mechanisms. Furthermore, this extensive numerical study highlighted the possible detrimental effect of the creep-ratchetting mechanism on the crack growth process. This work has a significant impact on structural integrity assessments of complex industrial components and for the better understanding of creep-fatigue lab scale tests.

Keywords; Creep-Fatigue interaction; Crack Initiation; Cyclic loading; Linear Matching Method.

Nomenclature

A Creep stress multiplier for the Norton equation.

A_1 Creep ductility multiplier.

B Creep stress multiplier for the Norton-Bailey equation.

B' Ramberg-Osgood material parameter.

B_1 Material property for creep ductility model in regime I.

B_2 Material property for creep ductility model in regime II.

D_c Total creep damage.

D_f Total fatigue damage.

D_{tot} Total damage.

d Grain size.

d_c^{DE} Creep damage per cycle based on Ductility Exhaustion.

d_c^{SMDE} Creep damage per cycle based on Stress Modified Ductility Exhaustion.

d_c^{TF} Creep damage per cycle based on Time Fraction rule.

eDSCA extended Direct Steady Cycle Analysis.

L Total number of load instances *l* within the eDSCA procedure.

LMM Linear Matching Method.

LMMF Linear Matching Method Framework.

K Total number of external sub-cycles *k* within the eDSCA procedure.

m Time exponent for the Norton Bailey equation.

m_1 Stress exponent of the stress dependent creep ductility.

n_1 Creep strain exponent of the stress dependent creep ductility.

n Stress exponent for the Norton equation.

$\dot{r}$ Rate of change of the cavity radius.

t_f Time to rupture.

t_h Creep Dwell Time

t_l Load instance *l* considered during the eDSCA procedure.

T Temperature of the material.

ΔG Creep activation energy.

Δt dwell time within the load instance during eDSCA.

$\Delta\varepsilon$ Strain range in the Ramberg-Osgood equation.

$\Delta\bar{\varepsilon}^c$ Equivalent creep strain increment within the eDSCA procedure.

$\Delta\varepsilon_{ij}^l$ Increment of strain at each n load instance within the eDSCA procedure.

$\Delta\rho_{ij,k+1}$ Residual stress increment associated to the increment of strain.

$\Delta\sigma$ Stress range in the Ramberg-Osgood equation.

$\dot{\bar{\varepsilon}}_c$ Equivalent creep strain rate.

$\bar{\varepsilon}_f$ Multi axial creep strain ductility.

ε_f Uniaxial creep strain ductility.

$\dot{\varepsilon}_{ij}^{c}$ Strain rate history within the eDSCA procedure.

$\dot{\bar{\varepsilon}}^{F}$ Creep strain rate obtained during the eDSCA procedure.

λ Load multiplier.

λ_c Cavity spacing.

$\bar{\mu}_k$ Iterative shear modulus at sub-cycle *k*.

$\bar{\rho}_{ij}$ Constant residual stress field.

ρ_{ij}^{r} Changing residual stress field

ρ_{ij}^{l} Total residual stress field at load instance *n*.

$\rho_{ij,k+1}(t_{l-1})$ Changing residual stress history of load instance *l-1*.

$\rho_{ij}^{r}\left(x,t_l\right)_k$ Sum of the constant residual stress field and all the previous changing residual stresses.

$\bar{\sigma}$ von Mises stress.

σ_1 Maximum principal stress.

σ_m Mean stress.

$\bar{\sigma}_s$ Equivalent stress at the start of the creep dwell.

$\bar{\sigma}_c$ Equivalent stress at the end of the creep dwell.

$\hat{\sigma}_{ij}$ Elastic stress solution.

$\hat{\sigma}_{ij}^{l}$ Elastic stress solution at *l* load instance.

$\sigma_y^R(x,t_l)_k$ Iterative von-Mises yield stress

1. Introduction

The reliability of components operating at high temperature under cyclic conditions is crucial for their safe and efficient operation. In the past twenty years significant research has been conducted on structures operating at high temperature. The main objective was to optimise and validate the effectiveness of methods for crack initiation and early crack growth in components subjected to both cyclic primary and secondary loads. A significant effort has been done to assess both creep-fatigue crack initiation and crack growth in rotor steel alloys [1-4]. The current assessment and design codes such as the UK's R5 procedures and the ASME Boiler and Pressure Vessel Code [5, 6], which are simplified methods, are capable of providing safe, but overly conservative predictions [7]. This conservatism is expected to be increased by the new operating conditions required for new high temperature reactors and power in-

dustry components[8, 9]. In the last decade, remarkable efforts have been made to accurately represent the viscous and plastic behaviour of materials subjected to cyclic load conditions at high temperatures. In addition to this, numerous research works on accurate creep damage modelling were conducted [10-14] by implementing the Continuum Damage Mechanics (CDM) approach in finite element analyses. Few researchers have concentrated on the creep-fatigue interaction and damage prediction using all the aforementioned techniques [15]. The use of these full inelastic analyses safely reduces the conservatism of rule-based methods. Despite this, they require numerous and precisely calibrated material parameters to guarantee accurate results. Moreover, they have a high computational cost, especially when 3D finite element models are considered. To assess the stabilised response of a structure, the Direct Cyclic Analysis (DCA) has recently been implemented within the commercial finite element software, ABAQUS [16]. This numerical method is capable of obtaining the stabilised cyclic response in an iterative way by using a combination of Fourier series and time integration of the nonlinear material response. However, it introduces numerical errors and convergence problems, meaning the DCA is not always a viable solution. In order to fill the gap between material science and industrial practical problems, direct methods such as the Linear Matching Method have been adopted, to calculate the steady state cycle that occurs rapidly in the life of the component without requiring too complex constitutive material model. The extended Direct Steady Cycle Analysis (eDSCA) has been developed to directly calculate the stabilised response of a structure subjected to a cyclic load at high temperature. In this study, the life of a Single Edge Notched Bend (SENB) specimen subjected to a cyclic mechanical load at constant high temperature is assessed using the updated LMM. To properly consider the effect of multiaxial stress state on the creep damage, for the first time the Stress Modified Ductility Exhaustion (SMDE) approach has been implemented within the eDSCA. The predicted endurances are compared with the experimental results obtained by Holdsworth [1] and Booth [7].

2. Strain Based method for creep damage modelling

2.1. Introduction to creep strain ductility under uni-axial load

When operating at high temperature several structural steels fail due to the growth and coalescence of voids. The mode of failure, as it was studied by Beere [17] and later by Hales [18], is dependent on the load level and the multiaxial stress state. In his early work, Hales identified that the strain to failure was related to the strain rate. Three distinct failure mechanisms or regimes have been identified and shown in Fig. 1a [19]. In his work Hales only considered spherical voids, with initial radius r_0, for simplicity. The failure occurs when the radius reaches the critical size of $\lambda/2$, where λ is the cavity spacing. Regime I, shown in Fig. 1b, occurs for high-stress level and the voids growth is the result of plastic deformation. An elegant mathematical representation is given by Hales, demonstrating how the failure strain is independent of stress and time. For a spherical cavity growing in a steady-state creep regime consider the following growth rate:

$$\dot{r} = B_1 \dot{\bar{\varepsilon}}_c \tag{1}$$

By integrating equation (1) the strain to failure is obtained:

$$\varepsilon_f = \dot{\bar{\varepsilon}}_c \cdot t_f = \frac{\lambda_c}{2B_1} \tag{2}$$

Equation (2) shows the existence of an upper-shelf for the creep ductility, and it can be obtained from hot tensile testing or high stress tensile creep testing. For intermediate stress levels, a transition is observed, Regime II in Fig. 1c. This change of mechanism between Regime I and II occurs when the

cavity growth for diffusion dominates over the plastic hole growth. In this regime the cavity radius growth rate is linearly related to the equivalent stress $\bar{\sigma}$ and the material parameter B_2:

$$\dot{r} = B_2 \bar{\sigma} \tag{3}$$

By integrating equation (3) the rupture time is given:

$$t_f = \frac{\lambda_c}{2B_2 \bar{\sigma}} \tag{4}$$

By combining equation (4) and the Norton law for steady-state creep, the strain to failure as a function of the strain rate, stress multiplier *A* and stress exponent *n* is given:

$$\varepsilon_f = \left(\frac{\lambda_c A^{\frac{1}{n}}}{2B_2} \right) \dot{\bar{\varepsilon}}_c^{\frac{(n-1)}{n}} = A_1 \dot{\bar{\varepsilon}}_c^{n_1} \tag{5}$$

Equation (5) shows how the strain to failure is a function of the strain rate, and it is related to both the material properties and load condition. However, when a low stress is applied the constrained diffusion mechanism dominates and Regime III starts as presented in Fig. 1d. For this regime, the strain to failure is represented by a constant value. The stress at cavitation boundaries relaxes, producing stress redistribution. This local mechanism stops when the local strain rate, due to the cavitation process, is equal to that present in the remote area. This physical behaviour can be expressed by the following equation, which is a fixed value function of the vacancy spacing λ and grain size *d*:

$$\varepsilon_f = \frac{\lambda_c \pi}{6d} \tag{6}$$

This physical and mathematical representation of the creep ductility can be used to estimate the creep damage in structures operating in creep regime. The so-called strain based methods have recently been further enhanced by Wen [20, 21] using a local approach based on scalar damage demonstrating good agreement. Equation (5) is the simplest definition of creep ductility used within the Ductility Exhaustion (DE) method, which has been extended by Spindler [22] to consider the effect of stress leading to the Stress Modified Ductility Exhaustion (SMDE) method. The creep damage per cycle is calculated by the following formulations for DE and SMDE respectively:

$$d_c^{DE} = \int_0^{t_h} \frac{\dot{\bar{\varepsilon}}_c}{\bar{\varepsilon}_f \left(\dot{\bar{\varepsilon}}_c, T \right)} dt \qquad d_c^{SMDE} = \int_0^{t_h} \frac{\dot{\bar{\varepsilon}}_c}{\bar{\varepsilon}_f \left(\dot{\bar{\varepsilon}}_c, \sigma_1, T \right)} dt \tag{7}$$

The contribution of the stress, which is neglected in DE, has been demonstrated by Spindler [22] to be important to better approximate the cavity nucleation process. Equation (5) has been extended to consider the effect of stress by the following equation:

$$\varepsilon_f = A_1 \cdot \exp\left(\frac{\Delta G}{RT} \right) \cdot \dot{\bar{\varepsilon}}_c^{n_1} \cdot \sigma_1^{-m_1} \tag{8}$$

Conversely, stress based methods that are widely adopted have drawbacks in terms of sensibility to the material parameters and stress levels. One of the most used is the Time Fraction (TF) defined as follow:

$$d_c^{TF} = \int_0^{t_h} \frac{dt}{t_f\left(\sigma, T\right)} \tag{9}$$

When the creep dwell starts at the maximum strain TF becomes overly conservative, and less conservative for small cyclic strain ranges.

2.2. The effect of stress and stress state on the creep ductility

The triaxial stress state has a significant impact on the failure of industrial components due to the presence of many cross-sectional area changes, grooves or welds. When creep and fatigue interact the damage caused by creep can be enhanced by the stress triaxiality $\sigma_m / \bar{\sigma}$. Due to this stress state the damage may develop inside the component, at a distance of several hundred microns from the stress concentrator as observed in notched specimens experiments[4, 23-25]. It has been further demonstrated by Spindler [26] , and recently by the review work done by Wen [19], how the stress triaxiality reduces significantly the creep ductility.

The MDF models can be divided into three categories: Physically Based, Semi-Empirical and Empirical MDFs. The first type incorporates the physical impact of multiaxial stress state to the creep fracture. The creep fracture is recognised to be governed by two mechanisms, the growth and the coalescence of micro voids. One of the most famous multiaxial ductility factors is the one created by Cocks and Ashby [27]. It is capable of modelling the grain-boundary cavity growth due to the creep power law of the surrounding matrix:

$$\frac{\varepsilon_f}{\bar{\varepsilon}_f} = \frac{\sinh\left[\frac{2}{3}\left(\frac{n-0.5}{n+0.5}\right)\right]}{\sinh\left[2\left(\frac{n-0.5}{n+0.5}\right)\right]\frac{\sigma_m}{\bar{\sigma}}} \tag{10}$$

As reported by Spindler [22] and recently by Wen [19] equation (10) becomes less effective for small changes of *n*, leading to overestimated values for the ductility. A significant enhancement has been done by [21] that introduced a new physically based MDF:

$$\frac{\varepsilon_f}{\bar{\varepsilon}_f} = \frac{\exp\left[\frac{2}{3}\left(\frac{n-0.5}{n+0.5}\right)\right]}{\exp\left[2\left(\frac{n-0.5}{n+0.5}\right)\right]\frac{\sigma_m}{\bar{\sigma}}} \tag{11}$$

Another physically based MDF is represented by the one developed by Spindler[22]. Two different cavity growth mechanisms are evaluated, the diffusion and the creep power law controlled growth. It has been demonstrated by Hales [18] that when the strain rate exponent n_1 in equation (8) is smaller than the theoretical one obtained by (n−1)/n, where n is the secondary creep stress exponent, the cavity growth mechanism is coupled with the diffusion and the creep power law mechanism. In this case, the modified Cavity Growth Factor (CGF) introduced is:

$$CGF_{\mathrm{mod}ified} = \frac{\bar{\sigma}}{\sigma_1}\exp\left(\frac{1}{2} - \frac{3\sigma_m}{2\bar{\sigma}}\right) \tag{12}$$

The first term of equation (12) $\left(\frac{\bar{\sigma}}{\sigma_1}\right)$ is used to properly describe the diffusion mechanism affected by the principal stress. The second term $\exp\left(\frac{1}{2} - \frac{3\sigma_m}{2\bar{\sigma}}\right)$ is used to model the creep power law cavity growth [28] and it is based on the model developed by Rice [29] for hole growth in the plastic deformation regime. To better evaluate the effect of multiaxial stress state on the creep ductility the plot of multiaxial ductility factor against the stress triaxiality is presented in Fig.2 . The uniaxial stress case is represented by a circle, all of the models presented pass from this point when the stress triaxiality is 0.33. All the experimental results available in the literature for a multiaxial stress state are present for stress triaxiality up to 1.6 [19]. It is worth mentioning that no cases are available for a low level of stress triaxiality below 0.33. This region is important and should be investigated more for its relevance in real practical cases. From Fig. 2 it is clear that the three physical methods give reasonable results. However, the most accurate are provided by the Spindler CGF and the newest developed by Wen and Tu. These two MDFs return very close results for stress triaxiality over 1.2. For stress triaxiality between 0.6 and 1.2, the Spindler CGF looks more accurate, especially for austenitic stainless steels and for CrMoV. Conversely, the MDF from Wen-Tu is more accurate for the others, providing a better lower-bound for 316H at a high level of triaxiality. However, it is still slightly insensitive to changes of stress exponent *n*. Due to the better performances of the Spindler CGF with the CrMoV and other structural steels, and its implementation within the UK's R5 procedure, it has been implemented within the LMM.

3. Creep-fatigue crack initiation procedure using the LMM

3.1. Assessing the steady state cycle and the creep damage

Consider an elastic perfect plastic material and the von Mises yield criterion $f\left(\sigma_{ij}\right) = 0$ with an associated flow rule a series of plastic mechanisms can be described by considering an applied load $\hat{\sigma}_{ij}$ and different load multipliers λ. These mechanisms include elastic shakedown, global shakedown and ratchetting. Global shakedown is defined when $f\left(\lambda\hat{\sigma}_{ij} + \bar{\rho}_{ij} + \rho_{ij}^{r}\right) \le 0$, where $\lambda\hat{\sigma}_{ij}$ is the scaled elastic solution and $\bar{\rho}_{ij}$ denotes a constant residual stress at the start and end of the loading cycle. Instead ρ_{ij}^{r} represents the changing residual stress field, which is calculated by the inelastic strain rate history. To ensure that ratchetting is not present the associated inelastic strain rate integrated over the cycle period must be zero.

When creep occurs within the steady state cycle, stress relaxation initiates and the yield function must be replaced by the creep flow stress, which depends on the creep strain rate calculated. In Fig. 3a the load history adopted in this work is shown, and it is divided into three load instances. It is assumed that the plastic or creep strains occur at fixed load instants, which better represent the entire load cycle. t_1 and t_3 represent points where the applied displacement changes introducing a residual stress field and a plastic strain increment (Fig. 3b). However, to introduce the creep dwell an additional load instance t_2 is necessary. After the loading step (t_1), creep will occur and the stress will relax. The elastic solution for that point is not compatible with the creep flow stress and a residual stress field will be calculated. For this residual stress field an associated creep strain increment is obtained. The stress

relaxation shown in Fig. 3b enhances the unloading phase (t_3), which exhibits an increase of the plastic strain.

The numerical procedure is based on the minimization of the following function, which is dependent on a class of kinematic admissible strain rate $\dot{\varepsilon}_{ij}^{c}$:

$$I\left(\dot{\varepsilon}_{ij}^{c}\right)=\sum_{l=1}^{L} I^{l} \tag{13}$$

where L is total number of loading instances considered, t_1,t_2, … t_L where plastic or creep strain are expected to occur. The minimization function can be formulated by using an incremental form:

$$I^{l}\left(\Delta\varepsilon_{ij}^{l}\right)=\int_{V}\left\{\sigma_{ij}^{l}\Delta\varepsilon_{ij}^{l}-\left[\hat{\sigma}_{ij}^{l}\left(t_{l}\right)+\rho_{ij}^{l}\left(t_{l}\right)\right]\Delta\varepsilon_{ij}^{l}\right\}dV \tag{14}$$

The residual stress $\rho_{ij}^{l}\left(t_{l}\right)$ at each load instance is calculated by the sum of the constant part of the changing residual stress $\bar{\rho}_{ij}$ and the summation of all the previous changing residual stress field increments $\Delta\rho_{ij}\left(t_{l}\right)$. This incremental formulation allows the strain rate history $\dot{\varepsilon}_{ij}^{c}$ to be replaced with a sequence of increments of strain $\Delta\varepsilon_{ij}^{l}$, which occur during the cycle at each time t_l.

The eDSCA is an iterative procedure that has been developed by Chen [30, 31] to calculate the inelastic strain increment $\Delta\varepsilon_{ij}^{l}$ to minimize the function shown in equation (14). This numerical procedure requires a total of K cycles to check the convergence of the minimization process. Within each k cycle a total of L sub-cycles need to be performed. For each loading instance l the associated residual stress field and inelastic strain increment are obtained. At each ABAQUS increment, both residual stress and inelastic strain are calculated for an associated elastic stress and the previous accumulated residual stresses. When considering a load instance t_l without creeping material, the inelastic strain increment $\Delta\varepsilon_{ij,k+1}(t_l)'$ can be evaluated for that load instance by;

$$\Delta\varepsilon_{ij,k+1}(t_l)'=\frac{1}{2\bar{\mu}(t_l)}\left[\hat{\sigma}_{ij}(t_l)+\rho_{ij,k+1}(t_{l-1})+\Delta\rho_{ij,k+1}(t_l)\right]' \tag{15}$$

where notation (') refers to the deviator component of stresses and $\bar{\mu}$ is the iterative shear modulus [30], $\hat{\sigma}_{ij}$ is the associated elastic solution, $\rho_{ij,k+1}(t_{l-1})$ is the prior changing residual stress history and $\Delta\rho_{ij,k+1}(t_l)$ is the residual stress associated to the inelastic strain increment. Within this iterative procedure it is possible to also consider the Ramberg-Osgood (RO) material response. The plastic strain calculated is used to iteratively change the yield stress in the upcoming *k+1* sub-cycle, simulating the hardening or softening of the material. When creep is considered, an effective creep strain $\Delta\bar{\varepsilon}^{c}$ is evaluated by adopting equation (16) for the associated dwell time Δt using the Norton Bailey relation:

$$\Delta\bar{\varepsilon}^{c}=\frac{B(n-1)\Delta t^{m+1}(\bar{\sigma}_{s}-\bar{\sigma}_{c})}{\left(\frac{1}{\bar{\sigma}_{c}^{n-1}}-\frac{1}{\bar{\sigma}_{s}^{n-1}}\right)(m+1)} \tag{16}$$

$\bar{\sigma}_c$ represents the creep flow stress, which is the sum of the start-of-dwell stress $\bar{\sigma}_s$ and the residual stress $\Delta\rho_{ij,k+1}(t_l)$ induced during the dwell period. The creep flow stress can be evaluated by considering the following equation, which relies on the accurate evaluation of the creep strain rate $\dot{\bar{\varepsilon}}^F$ at the end of the dwell time:

$$\bar{\sigma}_c = \left(\frac{\dot{\bar{\varepsilon}}^F}{B\Delta t^m} \right)^{\frac{1}{n}}$$
$$\dot{\bar{\varepsilon}}^F = \frac{\Delta\bar{\varepsilon}^c}{\Delta t} \frac{(m+1)}{(n-1)} \frac{\bar{\sigma}_c^n}{(\bar{\sigma}_s - \bar{\sigma}_c)} \left(\frac{1}{\bar{\sigma}_c^{n-1}} - \frac{1}{\bar{\sigma}_s^{n-1}} \right) \tag{17}$$

The stress and the creep strain rate fields obtained by the system of equations (17) are used to accurately calculate the uniaxial ductility and the CGF factor for each load instance where creep occurs using equations (8) and (12). The remaining part of the procedure calculates the residual stress at each increment through the solution of linear problems. At the end a residual stress field is obtained and the iterative shear modulus is updated for the next cycle *k+1* for each load instance t_l by adopting the linear matching equation;

$$\bar{\mu}_{k+1}(x,t_l) = \bar{\mu}_k(x,t_l) \frac{\sigma_y^R(x,t_l)_k}{\bar{\sigma}\left(\hat{\sigma}_{ij}(x,t_l) + \rho_{ij}^r(x,t_l)_k\right)} \tag{18}$$

where $\bar{\mu}_k(x,t_l)$ is the iterative shear modulus at the sub-cycle *k* for n^{th} load instance. $\sigma_y^R(x,t_l)_k$ is the iterative von-Mises yield stress for RO material model or yield stress for the Elastic Perfectly Plastic material model at load instance t_l. $\rho_{ij}^r(x,t_l)_k$ is the sum of the constant residual stress field and all the previous changing residual stresses at different load instances.

Once the whole procedure is converged the creep fatigue life of any component subjected to a cyclic thermal and mechanical load can be evaluated. All the required parameters for the assessment can be estimated from the steady state cyclic response obtained, using a similar procedure created by Wada[32]. The fatigue and creep damages per cycle are calculated separately by the accurate evaluation of total strain range, stress at the start of creep dwell, stress drop, creep strain rate and creep strain accumulated during the dwell.

4. Numerical case study: SENB

4.1. Finite element model and material properties

The same test specimen adopted by Holdsworth [1] has been used for this study. Due to the symmetry conditions only half of the entire model is analysed. The model is composed of 1425 plain strain quadrilateral elements, with a reduced integration scheme. As shown in Fig. 4, the mesh is refined near the round notch, which has a radius of 6 mm. Symmetry conditions are applied to the left side on the x-axis (Fig. 4), and the y translation is constrained with boundary conditions applied on the right part of the model. A Load Point Displacement (LPD) is imposed as shown in Fig. 4, producing the desired elastic stress field necessary to perform the LMM eDSCA analysis. The SENB specimen is subjected to different fully reversed LPDs in a 0.268 – 0.5 mm range, considering dwell time of 0, 0.5 and 16 hours. Another loading case is studied considering an additional pure axial load of 200 MPa.

The 1CrMoV material properties adopted for this work has been largely obtained from Japanese National Institute of Material Science (NIMS) database[33], and are shown in Table 1. The cyclic-stress strain behaviour of this alloy is modelled using the Ramberg-Osgood relationship:

$$\frac{\Delta\varepsilon}{2}=\frac{\Delta\sigma}{2E}+\left(\frac{\Delta\sigma}{B'}\right)^{\frac{1}{\beta}} \tag{19}$$

The Ramberg-Osgood constants are obtained by the locus of the tips of the steady state cycle response at 550 °C [34] for different total strain ranges. Due to the homogenous high temperature, the creep deformation that occurs during the dwell period is calculated using the Norton-Bailey relationship defined as:

$$\dot{\bar{\varepsilon}}_c = B\cdot\bar{\sigma}^{n}\cdot t^{m} \tag{20}$$

To calculate the most accurate creep damage, the creep uniaxial ductility is calculated. To avoid overly conservative results, the local rupture strain is calculated by the reduction of area measured during the creep test [1]. The data used for the material property extrapolation has been obtained from the NIMS database[33]. A total of 10 different batches of data are used to fully describe the material ductility, for high strain rate the hot tensile results are used. Both DE and SMDE parameters are reported in Table 3. The fatigue data is obtained from the R66 Issue 8 [35] database, for 1CrMoV at 550 °C. The data are obtained from isothermal low cycle fatigue tests at different strain ranges. The number of cycles to failure is defined as the number of cycles required to obtain a 2% stress drop in the steady state cycle.

The fatigue damage per cycle is obtained by $d_f = 1/N_0$, where N_0 is the cycle to failure associated with the total strain range calculated by the eDSCA. Creep damage (d_c) per cycle can be calculated with both stress or strain based methods. When TF rule is used the average creep stress during the dwell is obtained to determine the rupture time required by equation (9). Conversely, for DE and SMDE the creep strain increment and the multiaxial creep ductility are calculated for the associated creep dwell. Hence, the total damage per cycle is defined as the linear sum of fatigue and creep damages, subsequently the predicted endurance is defined as $N_f = \left(d_f + d_c\right)^{-1}$. By knowing the experimental endurance for each load case, the total damage based on the total creep damage D_c and total fatigue damage D_f can be calculated. D_{tot} must be lower than unity to prevent crack initiation, otherwise the component is likely to exhibit crack initiation. The unity limit is an empirical rule, and it is based on direct comparison with experimental results [34].

5. Results and discussions

5.1. Predicted endurance by LMM

A benchmark test has been performed to identify discrepancies between the different creep damage models. A total of four cases have been analysed, one without creep and three with creep dwell at different positions within the load cycle (Table 5). The stress relaxation caused by creep tends to increase the fatigue damage per cycle. The creep damage calculated by the TF gives the most conservative results for high levels of stress at the start of the tensile dwell. However, it is capable of identifying the compressive dwell producing negligible damage. Conversely, the DE method predicts overly optimistic results for the first case and overly conservative for the latter. The SMDE performs very well in all the cases considered, combining the strengths of both stress and strain based methods. For these reason, only DE and SMDE methods will be used for the study.

The results obtained are summarised in Fig. 5, where the observed number of cycles to failure are plotted against those predicted by different approaches. The continuous line represents the interpolation of the observed experimental endurances (solid square) due to different loading conditions. The LMM predictions are plotted for different dwell times, loading conditions and creep damage models. The results for DE and SMDE are represented by diamonds and circles respectively. A good agreement is obtained by the SMDE for most of the analysed cases. Conversely, DE has been demonstrated to be slightly non-conservative but always within a factor of 2. Accurate predictions are obtained for long creep dwell (16 hours) by the SMDE. These endurances predicted are never less conservative than the observed ones, except for one single case. For all the analysed cases, the predicted cycles to failure are never more conservative than those calculated by the R5 Procedures. Very good accuracy is demonstrated when a superimposed load of 200 MPa and a dwell time of 0.5 hours are considered. For this case, the life predicted by the LMM is 661 and 570 cycles for DE and SMDE respectively, which is very close to that observed (576 cycles). The solution obtained is significantly more accurate than the R5 procedures (108 cycles) and comparable to the fully inelastic analysis (526 cycles).

Creep and fatigue damage per cycle are plotted against the load applied for different dwell times in Fig. 6. Both the damages are shown in Fig. 6a for a dwell time of 0.5 hour, showing a strong creep-fatigue interaction for a total LPD between 0.45 and 0.55 mm. For low strain case (small LPD) creep damage is dominant over fatigue and this is reversed for high strains. This behaviour completely changes for longer dwell times, as is shown in Fig. 6b where the creep damage per cycle is always greater than fatigue.

When creep damage dominates the failure is expected to initiate at a depth of several hundred micro-meters from the notch surface as highlighted in Fig. 7, where the contour of the total damage per cycle is shown for two dwell times at the same mechanical load. By comparing Fig. 7a and Fig. 7b it is evident how creep dominated failures initiates in a deeper area (Fig. 7a), rather than being confined to the surface as for fatigue driven one. In Fig. 8 the stress state and the triaxiality factor is plotted against the cross section of the notched specimen. The creep damage contour calculated is superimposed to the plot. The von Mises stress at the start of the creep dwell is subjected to a large relaxation. As expected the principal stress is larger than the von Mises stress and the triaxiality factor is remarkably higher inside the bar. In that location, as depicted by Fig. 8, the maximum damage per cycle is observed, which is about 1000 micrometres from the surface as observed by many experimental and numerical works on notched specimens[23-25].

A parametric study has been performed to investigate the effect of the superimposed primary load on the component's response, considering a 0.5 hour creep dwell, a total LPD of 0.8 mm and an increasing superimposed load of 50, 100, 150, 200, 250 and 300 MPa. Up to 200 MPa the failure is always dominated by creep and fatigue interaction. However, creep ratchetting develops but it still negligible. The total damage per cycle produced by the creep-fatigue interaction, the creep-fatigue and the creep ratchetting endurances are reported in Fig. 9. For the superimposed load of 100 MPa creep-fatigue interaction dominates, with a predicted life of 542 and 1360 cycles for creep-fatigue and creep ratchetting respectively. For the 200 MPa load case the predicted life due to the two mechanisms is comparable and affect two close areas in the notch groove as shown in Fig. 9. If the axial load is increased up to 300 MPa the response changes and the predicted cycles to failure due to creep-ratchetting is 117 against the 344 of creep-fatigue mechanism. The locations where the damages initiate do not coincide, but are close enough to be likely to interact especially during the crack growth process. The superimposed primary load as expected reduces the component life and introduces an incremental mechanism, which affects the notch root area. Tong [36, 37] introduced and demonstrated that the ratchetting at the crack tip is a driving mechanism for the crack growth process. The notch can be divided into three distinct areas: i) creep fatigue dominated, ii) creep-fatigue and creep ratchetting interaction area and iii) creep ratchetting dominated area. If a crack initiates in the second area the

concept introduce by Tong[36] becomes relevant. The surrounding material ahead the crack exhibits creep-ratchetting affecting also secondary cracks, leading to a much more complex scenario in terms structural integrity of the defective body.

A final overview of all the results obtained is given in Fig. 10, where the creep fatigue linear damage summation diagram is shown. All the predicted endurances, except three, are in the crack initiation area as expected (Fig. 10). Three failure mechanisms can be identified, fatigue dominated (above the dot-dash line), creep dominated (below the dot-dash line) and creep fatigue interaction for points that lay closer to the limit (dot-dash line). For the first type, transgranular cracking is predicted to initiate from the surface of the notched area, and the mechanism is strongly affected by the total strain range. Instead, the second one exhibits intergranular damage, which initiates inside the specimen and the principal stress is the driving parameter. In the last case, the interaction between creep and fatigue is more complex and both surface and interior cracking are expected.

To further verify the accuracy of the adopted method, a comparison between metallographic inspections on experimental results obtained by Holdsworth [38] and the numerical prediction has been presented in Fig. 11. Fig. 11a shows the multiple crack initiation occurred in the SENB component subjected a fully reversed total LPD of 0.8 mm, and the superimposed load of 200 MPa with a dwell time of 0.5 hour. The damage develops from the surface of the specimen, demonstrating that the crack initiation is fatigue driven. This failure mechanism has been identified by the numerical solution and the load point (square) shown in Fig. 10 is largely within the fatigue dominated area. Furthermore, Fig. 11b shows the area of maximum damage, which is comparable to the area where multiple cracks have occurred.

6. Conclusions

In this work, the LMM eDSCA method has been successfully improved by improved by implementing the Stress Modified Ductility Exhaustion delivering a study on the creep-fatigue interaction Single Edge Notch Bend specimen. The cyclic response has been identified and discussed pointing out its implication on the structural integrity. The main results obtained within this research work are as follow:

1. Implementing the Stress Modified Ductility Exhaustion approach with the Cavity Growth Factor into the eDSCA leads to very accurate life predictions. Excellent agreement has been demonstrated for cyclic loads when a primary load is introduced. All the failure mechanisms have been properly identified and match with the experimental observations available in the literature.

2. The physical effect of the associated load level on the crack initiation mechanism has been properly modelled with the proposed numerical procedure. Load levels confirmed to be important in influencing the type of failure mechanism. Furthermore, the stress triaxiality, which has a severe effect on creep ductility, has been investigated and modelled properly.

3. A new and more detailed numerical study has been performed varying the superimposed primary load. For a superimposed primary load up to 200 MPa the creep-fatigue crack initiation dominates. Conversely, the failure is driven by creep-ratchetting affecting a different location. For this specific case creep-ratchetting is expected to enhance the crack growth process.

4. The results obtained further demonstrate the capabilities of direct methods, such as the LMM, in assessing structures subjected to cyclic loading conditions when a limited number of experimental data is available.

Acknowledgements

The authors gratefully acknowledge the support of the University of Strathclyde, the Royal Society (IE140842), the International Cooperation and Exchange Project NSFC (11511130057) and the National Science Foundation for Distinguished Young Scholars of China (11325211) during the course of this work. Further acknowledgments are expressed to Dr Spindler of EDF Energy, Dr Holdsworth of EMPA for sharing their previous research works and providing support throughout this research.

List of tables

Table 2 Material properties for elastic, plastic and creep behaviour.

1CrMoV at 550 °C		
Young's modulus	151700 MPa	
Poisson's ratio	0.3	
Ramberg-Osgood parameters	$B^{'}$ = 646.67 MPa	β = 0.1092
Norton Bailey parameters	B = 2.5E-30 n = 10.5	m = -0.6

Table 4 Parameters for DE and SMDE creep ductility models.

DE	SMDE
A_1 = 19.005	A_1 = 1.5489
n_1 = 0.3489	n_1 = 0.2953 m_1 = 0.2111

Table 6 Fatigue and creep damages calculated for different loading cycles of SENB specimen subjected to a total displacement of 0.8 mm and a dwell time of 0.5 hours at 550 °C.

Load cycle	Fatigue damage	Creep damage		
		DE	SMDE	TF
Pure fatigue	$1.030 \cdot 10^{-3}$	-	-	-
Tensile peak dwell	$1.097 \cdot 10^{-3}$	$3.19 \cdot 10^{-4}$	$5.57 \cdot 10^{-4}$	$1.92 \cdot 10^{-2}$
Compressive peak dwell	$1.099 \cdot 10^{-3}$	$3.36 \cdot 10^{-3}$	$2.17 \cdot 10^{-7}$	$2.06 \cdot 10^{-6}$
Tensile and compressive dwell	$1.182 \cdot 10^{-3}$	$3.32 \cdot 10^{-3}$	$1.03 \cdot 10^{-3}$	$1.92 \cdot 10^{-2}$

List of figures

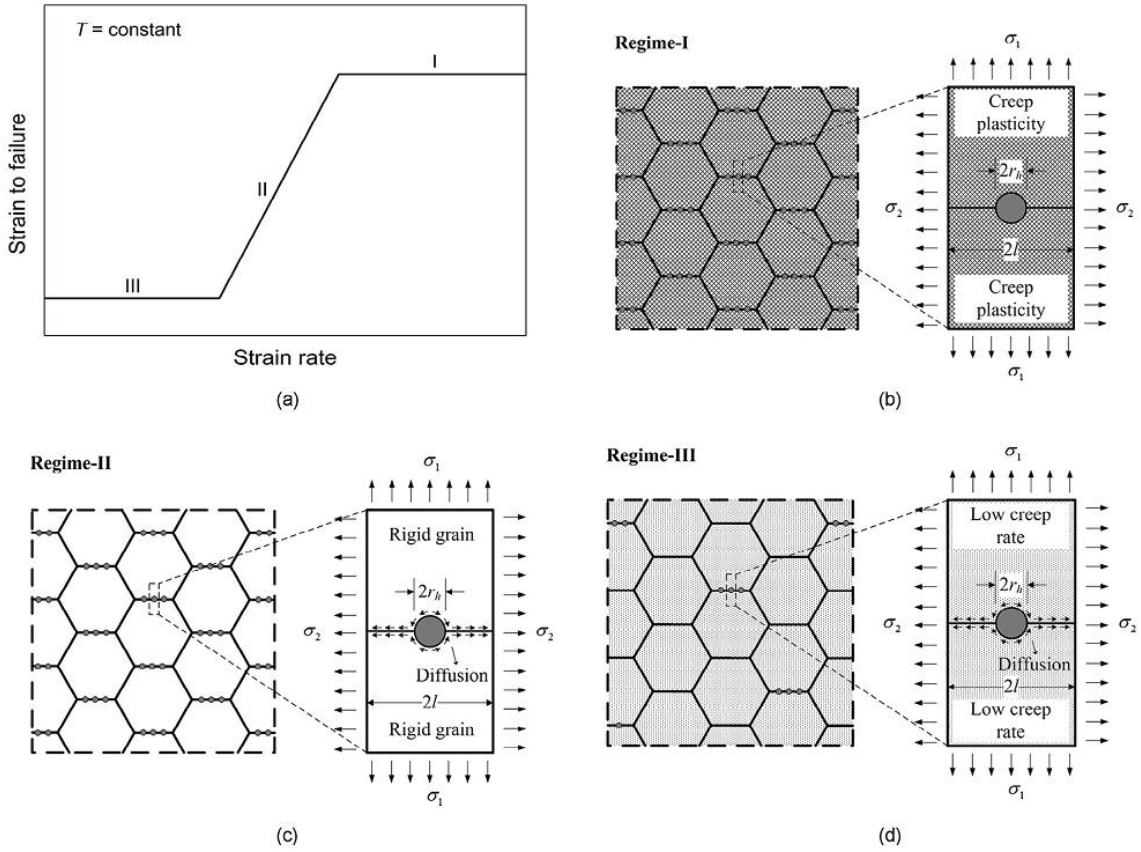

Fig. 1 Effect of strain rate on the failure ductility. a) Schematic representation of the three regimes depending on the creep strain rate, b) regime-I where plastic cavity growth dominates, c) regime-II where diffusion controlled cavity growth occurs, d) regime-III where constrained diffusion growth takes place. (Source: Wen et all. [19])

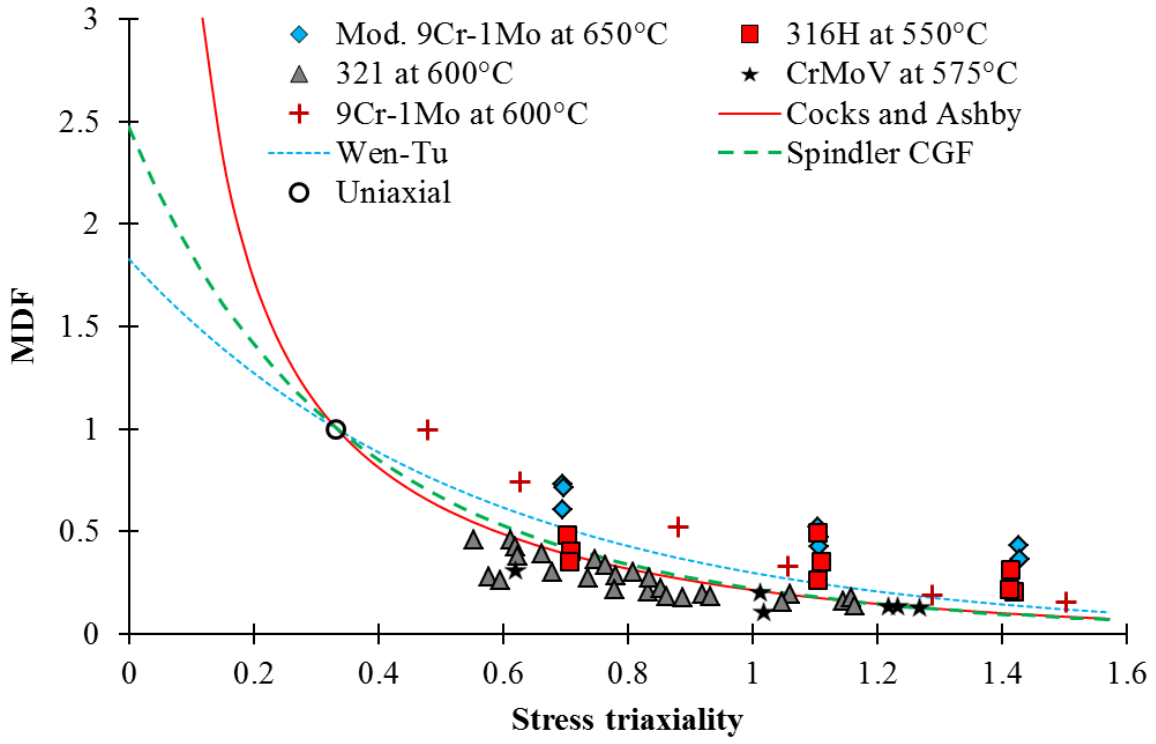

Fig. 2 Effect of stress triaxiality on the Multiaxiality Ductility Factor (MDF) for different physical based models. The plot of MDFs and experimental results [3, 23, 39-41] on notched bar specimens at high temperature are plotted against the stress triaxiality.

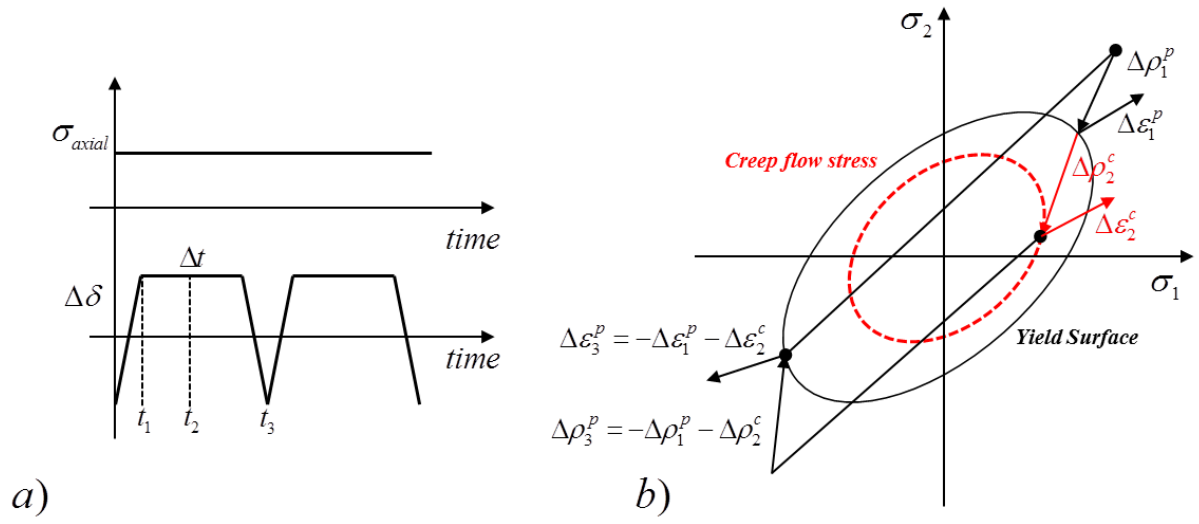

Fig. 3 Diagrammatic representation of load history and material response to the cyclic load. a) Load history with a creep dwell, b) schematic representation of the quantities involved within the loading cycle.

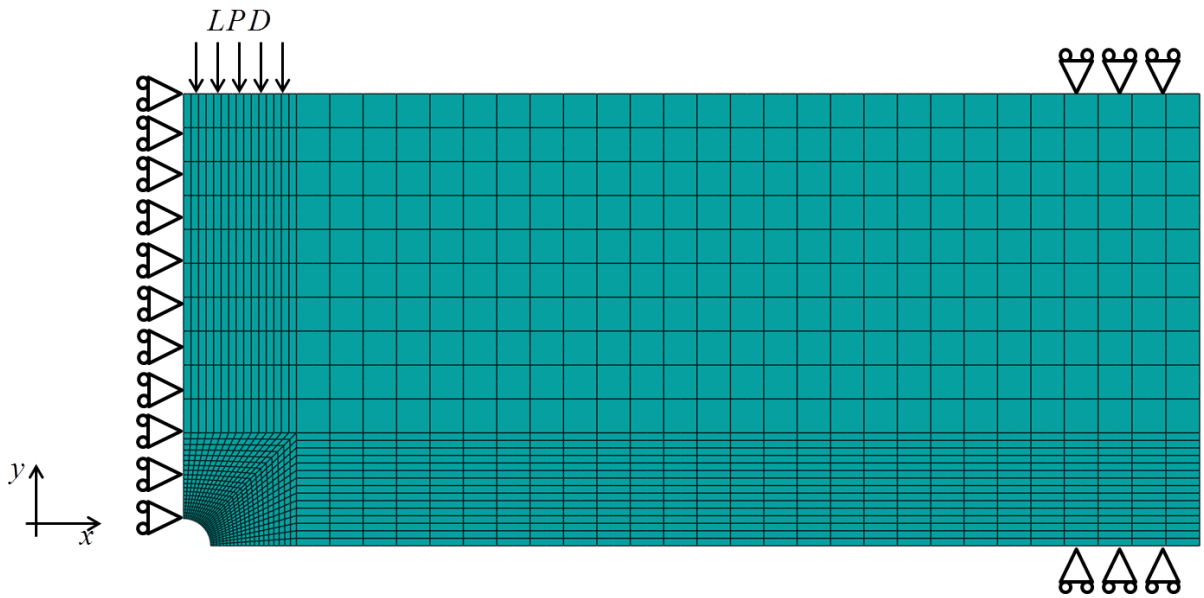

Fig. 4 Numerical model of the Single Edge Notched Bar (SENB). Load Point Displacement (LPD) and boundaries conditions are shown, a refined mesh has been used for the area close to the notch.

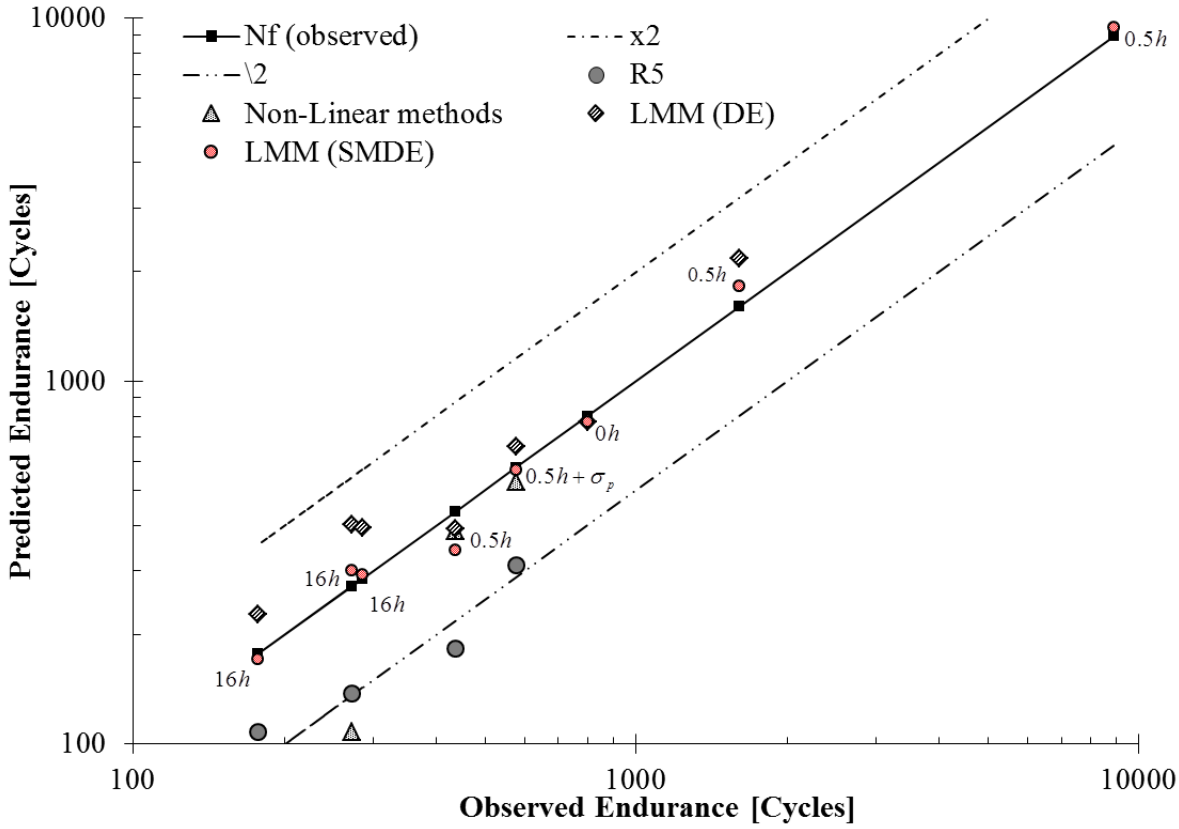

Fig. 5 Endurance plot for all the cyclic cases considered. The plot depicts the experimental cycles to failure (solid square), the LMM predictions (diamond, and circle), R5 predictions (solid circle), inelastic analyses prediction (triangle) for different dwell times and applied loads.

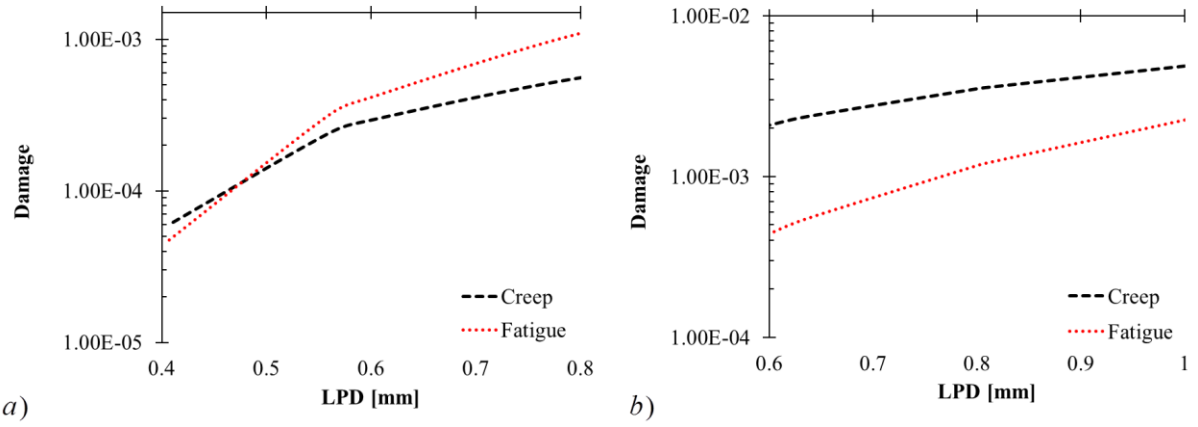

Fig. 6 Creep and fatigue damage per cycle for different Load Point Displacement applied for a dwell time of a) 0.5 and b) 16 hours.

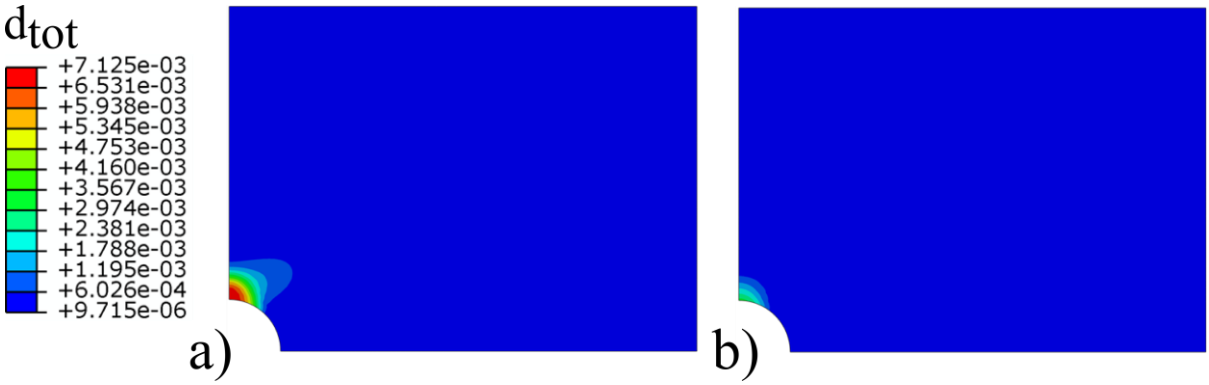

Fig. 7 Contours showing the combined effect of creep and fatigue damage. Total damage per cycle calculated for an applied LPD of 1.0 mm at a) 16 hours and b) 0.5 hour creep dwell.

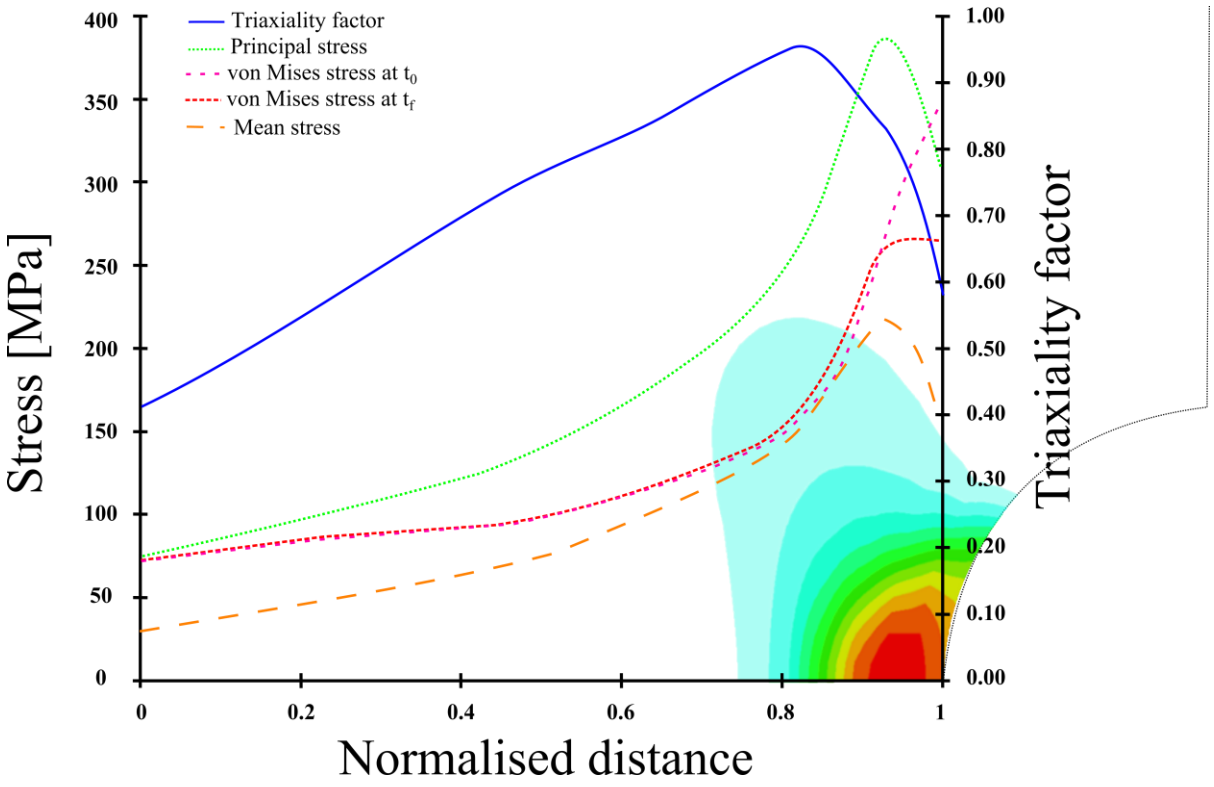

Fig. 8 Impact of stress state on creep damage. Stress and triaxiality factor distribution in the cross section of the notched specimen and superimposed contour of the creep damage for a LPD of 1.0 mm and a dwell time of 16 hours.

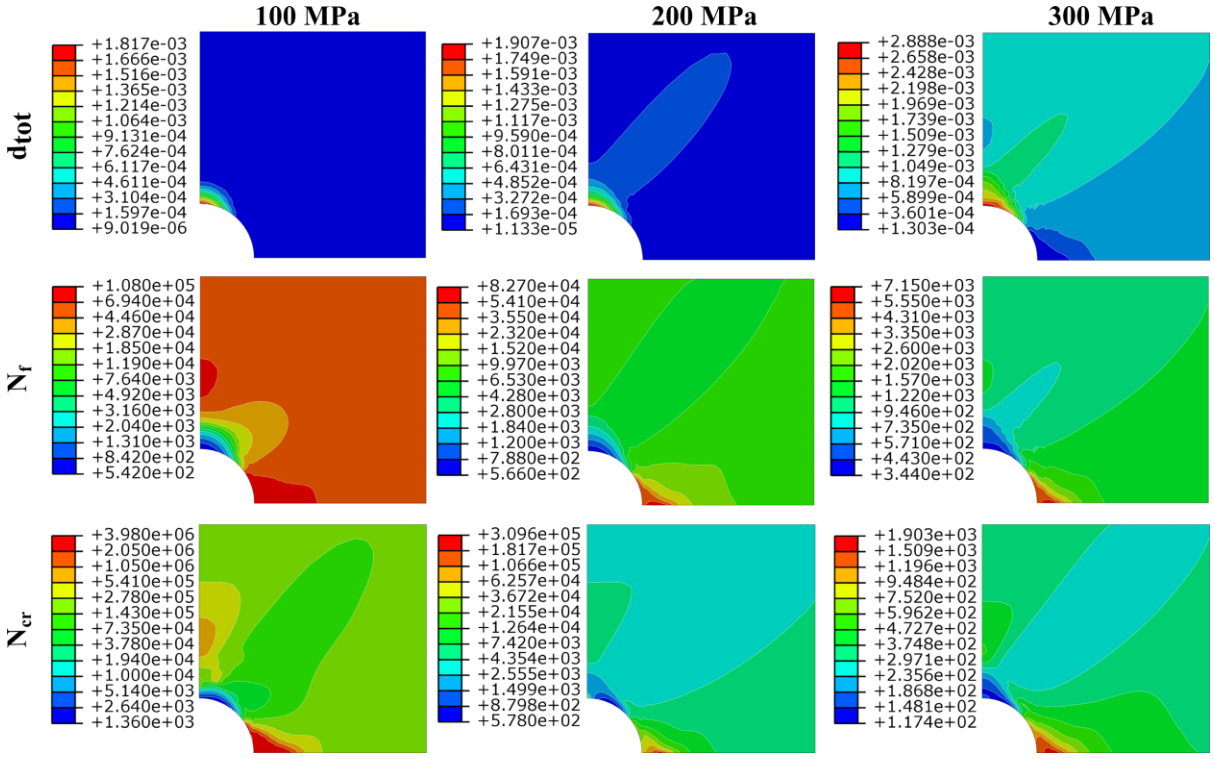

Fig. 9 Contours of total damage per cycle, creep-fatigue life and creep-ratchetting life for a superimposed primary load of 100, 200 and 300 MPa.

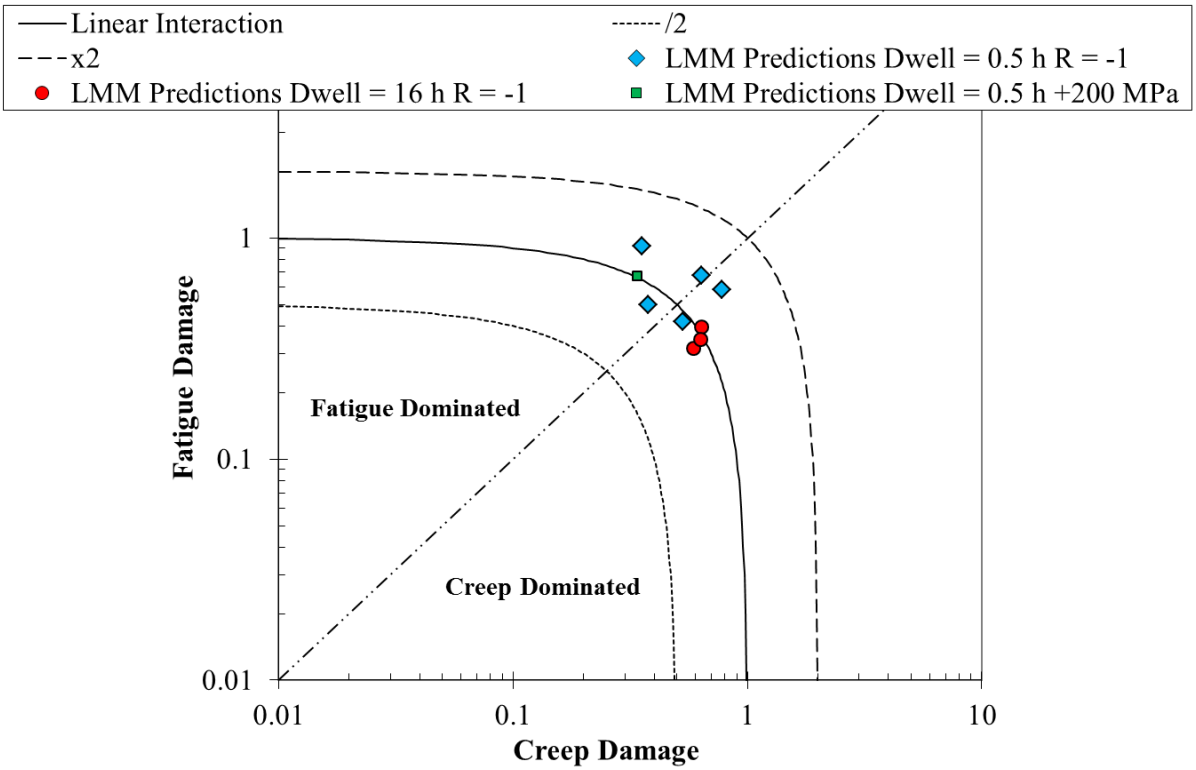

Fig. 10 Damage interaction diagram for the cyclic loading conditions exanimated by LMM and SDME.

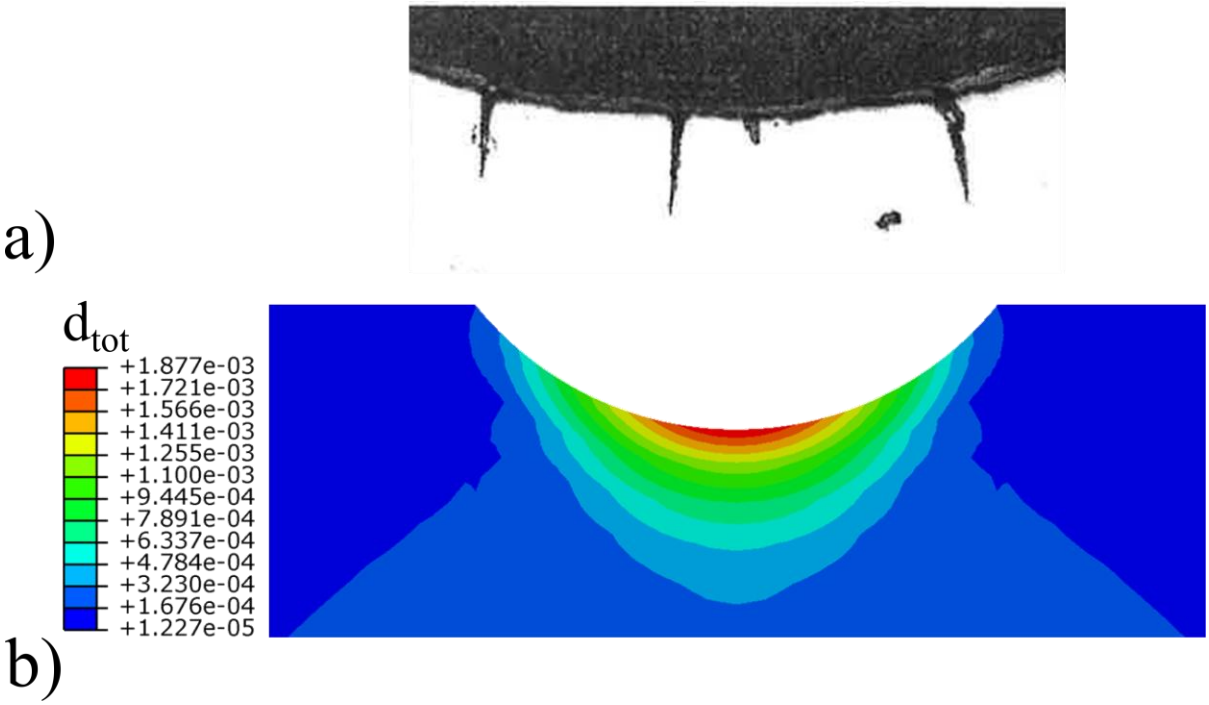

Fig. 11 Comparison between experimental result and numerical prediction. a) Creep-fatigue crack initiation and "early" growth at groove root for 1CrMoV SENB specimen [38], and b) total damage per cycle calculated by the LMM for a 0.4 mm displacement and a superimposed primary load of 200 MPa, with a dwell time of 0.5 hour.

References

1. Holdsworth S.R. (1996) Prediction of creep-fatigue behaviour at stress concentrations in 1CrMoV rotor steel. *Conference on Life Assessment and Life Extension of Engineering Plant, Structures and Components*, Churchill College, Cambridge, 137-146.
2. Holdsworth SR, Skelton RP, Dogan B (2010) Code of practice for the measurement and analysis of high strain creep-fatigue short crack growth. *Materials at High Temperatures*. **27**: 265-283.
3. Isobe N, Yashirodai K, Murata Ki (2014) Creep damage assessment for notched bar specimens of a low alloy steel considering stress multiaxiality. *Engineering Fracture Mechanics*. **123**: 211-222.
4. Holdsworth S (2015) Creep-Fatigue Failure Diagnosis. *Materials*. **8**: 5418.
5. The American Society of Mechanical Engineers (2013) *ASME boiler & pressure vessel code : an international code, Division 1 - Subsection NH*.
6. EDF Energy (2014) *Assessment procedure for the high temperature response of structures, R5 Issue 3*.
7. Booth P, Budden PJ, Bretherton I, Bate SK, Holdsworth (1997) Validation of the shakedown route in R5 for the assessment of creep fatigue crack initiation. *Structural Mechanics in Reactor Technology (SMiRT 14)*, Lyon, France.
8. Sabharwall P, Bragg-Sitton SM, Stoots C (2013) Challenges in the development of high temperature reactors. *Energy Conversion and Management*. **74**: 574-581.
9. Weitzel PS, Tanzosh J, Boring B, Okita N, Takahashi T, Ishikawa N (2012) Advanced Ultra-Supercritical Power Plant (700 to 760 °C) Design for Indian Coal. *Power-Gen Asia, Bangkok, Thailand*.
10. Naumenko K, Kutschke A, Kostenko Y, Rudolf T (2011) Multi-axial thermo-mechanical analysis of power plant components from 9–12% Cr steels at high temperature. *Engineering Fracture Mechanics*. **78**: 1657-1668.
11. Naumenko K, Altenbach H, Gorash Y (2009) Creep analysis with a stress range dependent constitutive model. *Archive of Applied Mechanics*. **79**: 619-630.
12. Dyson B (2000) Use of CDM in materials modeling and component creep life prediction. *Journal of pressure vessel technology*. **122**: 281-296.
13. Hyde T, Xia L, Becker A (1996) Prediction of creep failure in aeroengine materials under multi-axial stress states. *International journal of mechanical sciences*. **38**: 385-403.
14. Hayhurst D, Lin J, Hayhurst R (2008) Failure in notched tension bars due to high-temperature creep: Interaction between nucleation controlled cavity growth and continuum cavity growth. *International Journal of Solids and Structures*. **45**: 2233-2250.
15. Wang W, Buhl P, Klenk A, Liu Y (2015) Study of creep–fatigue behavior in a 1000 MW rotor using a unified viscoplastic constitutive model with damage. *International Journal of Damage Mechanics*.
16. Hibbitt D, Karlsson B, Sorensen P (2012) Abaqus 6.12. 3 Manual.
17. Chen I-W, Argon A (1981) Diffusive growth of grain-boundary cavities. *Acta Metallurgica*. **29**: 1759-1768.
18. Hales R (1994) The role of cavity growth mechanisms in determining creep-rupture under multiaxial stresses. *Fatigue & Fracture of Engineering Materials & Structures*. **17**: 579-591.
19. Wen J-F, Tu S-T, Xuan F-Z, Zhang X-W, Gao X-L (2016) Effects of Stress Level and Stress State on Creep Ductility: Evaluation of Different Models. *Journal of Materials Science & Technology*.
20. Wen J-F, Tu S-T, Gao X-L, Reddy J (2013) Simulations of creep crack growth in 316 stainless steel using a novel creep-damage model. *Engineering Fracture Mechanics*. **98**: 169-184.
21. Wen J-F, Tu S-T (2014) A multiaxial creep-damage model for creep crack growth considering cavity growth and microcrack interaction. *Engineering Fracture Mechanics*. **123**: 197-210.
22. Spindler MW (2007) An improved method for calculation of creep damage during creep–fatigue cycling. *Materials Science and Technology*. **23**: 1461-1470.

23. Goyal S, Laha K, Mathew MD (2014) Creep Life Prediction of Modified 9Cr-1Mo Steel under Multiaxial State of Stress. *Procedia Engineering*. **86**: 150-157.
24. Isobe N, Yashirodai K, Murata Ki (2015) Creep Damage Assessment Considering Stress Multiaxiality for Notched Specimens of a CrMoV Steel. *ICMFF10*.
25. Takahashi Y (2010) Comparison of notched bar creep behavior of various alloys. *ASME 2010 Pressure Vessels and Piping Division/K-PVP Conference*. American Society of Mechanical Engineers, 485-491.
26. Spindler M (2004) The multiaxial creep ductility of austenitic stainless steels. *Fatigue & Fracture of Engineering Materials & Structures*. **27**: 273-281.
27. Cocks A, Ashby M (1980) Intergranular fracture during power-law creep under multiaxial stresses. *Metal science*. **14**: 395-402.
28. Hellan K (1975) An approximate study of void expansion by ductility or creep. *International Journal of Mechanical Sciences*. **17**: 369-374.
29. Rice JR, Tracey DM (1969) On the ductile enlargement of voids in triaxial stress fields. *Journal of the Mechanics and Physics of Solids*. **17**: 201-217.
30. Chen H, Chen W, Ure J (2014) A Direct Method on the Evaluation of Cyclic Steady State of Structures With Creep Effect. *Journal of Pressure Vessel Technology*. **136**: 061404-061404.
31. Chen H, Ponter AR (2006) Linear Matching Method on the evaluation of plastic and creep behaviours for bodies subjected to cyclic thermal and mechanical loading. *International Journal for Numerical Methods in Engineering*. **68**: 13-32.
32. Wada Y, Aoto K, Ueno F (1997) Creep-fatigue evaluation method for type 304 and 316FR SS.
33. NIMS (1990) NIMS creep data sheet 44: Data sheets on the elevated-temperature properties of 1Cr-1Mo-0.25V steel forgings for turbine rotors and shafts (ASTM A470-8).
34. Skelton R (2012) *High temperature fatigue: properties and prediction*. Springer Science & Business Media.
35. EDF Energy (2011) *AGR Materials Data Handbook R66 Revision 9*.
36. Tong J, Zhao LG, Lin B (2013) Ratchetting strain as a driving force for fatigue crack growth. *International Journal of Fatigue*. **46**: 49-57.
37. Tong J, Lin B, Lu YW, et al. (2015) Near-tip strain evolution under cyclic loading: In situ experimental observation and numerical modelling. *International Journal of Fatigue*. **71**: 45-52.
38. Holdsworth S (1998) Creep-fatigue crack growth from a stress concentration. *Materials at high temperatures*. **15**: 111-116.
39. Oh C-S, Kim N-H, Kim Y-J, Davies C, Nikbin K, Dean D (2011) Creep failure simulations of 316H at 550 C: Part I–A method and validation. *Engineering Fracture Mechanics*. **78**: 2966-2977.
40. Yoshida K, Yatomi M (2011) Creep damage evaluation for HAZ of Mod. 9Cr-1Mo steels under multi-axial stress conditions. *Procedia Engineering*. **10**: 490-495.
41. Allais L, Auzoux Q, Reytier M, Pineau A (2005) Fissuration en relaxation des jonctions soudées en aciers inoxydables austénitiques. *Mécanique & Industries*. **6**: 45-54.